Journal of Power Sources 196 (2011) 3310–3316

Contents lists available at ScienceDirect

Journal of Power Sources

journal homepage: www.elsevier.com/locate/jpowsour

Electrochemical performance of highly mesoporous nitrogen doped carbon cathode in lithium–oxygen batteries

Padmakar Kichambare[a], Jitendra Kumar[b], Stanley Rodrigues[a,*], Binod Kumar[b]

[a] Air Force Research Laboratory, Propulsion Directorate, Wright-Patterson Air Force Base, OH 45433-7252, United States
[b] Electrochemical Power Group, University of Dayton Research Institute, 300 College Park, Dayton, OH 45469-0170, United States

ARTICLE INFO

Article history:
Received 30 September 2010
Received in revised form 8 November 2010
Accepted 22 November 2010
Available online 26 November 2010

Keywords:
Nitrogen doped mesoporous carbon
Lithium–air
Electrochemical impedance spectroscopy
Discharge cell capacity
Solid-state lithium–oxygen battery

ABSTRACT

Nitrogen doped carbon with a high surface area was used as cathode electrode in a solid-state lithium–oxygen battery. Various techniques including the Brunauer–Emmett–Teller (BET) surface area, X-ray diffraction (XRD), thermogravimetric analysis (TGA), scanning electron microscopy (SEM) and energy dispersive X-ray analysis (EDX) were employed to evaluate the nitrogen functionality on carbon. The electrochemical properties of nitrogen doped carbon as cathode electrode in lithium–oxygen battery were studied using galvanostatic charge–discharge characteristics and electrochemical impedance spectroscopy (EIS). The lithium–oxygen cell fabricated with nitrogen doped Ketjenblack–Calgon activated carbon cathode exhibits two times higher discharge cell capacity than that of a cathode composed of only Ketjenblack–Calgon activated carbon. This work shows that the nitrogen functionality on carbon is responsible for the electro-catalytic activity of cathode and an enhancement in cell capacity of lithium–oxygen battery.

Published by Elsevier B.V.

1. Introduction

Metal–air batteries have garnered attention as potential high performance lightweight power sources for electronic devices [1]. Among metal–air batteries, lithium–air batteries offer the most promise for extremely high persistence applications [2,3]. These batteries have significant advantages over conventional electrochemical energy storage devices [4] because of their high specific capacity. Abraham and Jiang [5] demonstrated the first non-aqueous, rechargeable lithium–oxygen cell that was based upon metallic lithium anode, polymer electrolyte separator, and a carbon-impregnated solid-polymer electrolyte composite cathode with gravimetric capacity of 1410 mAh g^{-1} in pure oxygen atmosphere. Even higher cathode capacity of 2120 mAh g^{-1} for lithium–air cell is reported by Read et al. [6] and the improved cell capacity is due to the designing of air cathodes capable of sustaining higher oxygen concentrations. Cathode capacity approaching 4000 mAh g^{-1} for a Mn based catalyst [7] and cathode capacity 5360 mAh g^{-1} for cell employing a hydrophobic ionic liquid and lithium salt were reported [8]. A gravimetric capacity of 5813 mAh g^{-1} was achieved using a novel lithium–oxygen cathode architecture without the use of catalyst [9]. Although large gravimetric capacities are obtained, the current density is small. Bruce and co-workers reported a rechargeable lithium–oxygen battery using Li_2O_2 and $LiCoO_2$ electrodes [10,11]. They report Li_2O_2 decomposes to yield $Li + O_2$ on electrochemical charging and that the charge/discharge cycling is sustainable for many cycles. To improve the capacity of lithium–oxygen battery, various approaches in lithium–oxygen cell architecture were reported, for example the use of bi-layer carbon electrode consisting of an active and diffusion layers [12], different carbon sources [13], superfine platinum particles [14] and bi-functional platinum–gold nanoparticles loaded onto carbon [15].

In our most recent studies, a fully solid-state, rechargeable lithium–oxygen battery [16] with an excellent thermal stability and re-chargeability in the 30–105 °C temperature range was reported. The cell was subjected to 40 charge–discharge cycles at current densities ranging from 0.05 to 0.25 mA cm^{-2}. Since our approach to fabricate a totally solid-state and rechargeable lithium–oxygen battery is easily scalable, such a battery holds great potential for realization of commercially viable, safe and lighter lithium–oxygen batteries for applications ranging from electric cars to unmanned aerial vehicles. Although these batteries are of considerable interest, their active life is limited by the diffusion and reduction of oxygen in the cathode. The performance of the cathode in these batteries is a major limiting factor in optimizing the power output. To enhance the performance of the cathode, it is of interest to investigate nitrogen doped carbon to enhance the oxygen reduction reaction activity. The doping of the carbon with nitrogen atoms has drawn much attention because conjugation between the nitrogen lone-pair electrons and graphene π-systems [17–19] may create nanostructures with desired properties. Recently, the nitrogen

* Corresponding author. Tel.: +1 937 255 2848; fax: +1 937 656 7529.
E-mail address: Stanley.Rodrigues@wpafb.af.mil (S. Rodrigues).

0378-7753/$ – see front matter Published by Elsevier B.V.
doi:10.1016/j.jpowsour.2010.11.112

doped carbon nanoparticles exhibited a good support for anchoring platinum nanoparticles than carbon XC-72 [20,21]. Importantly, the nitrogen doping of carbon materials has been shown to improve the activity of carbon for oxygen reduction [22–24]. Furthermore, the mesoporous carbon with high porosity is expected to facilitate the access of oxygen to the reaction sites inside the pores of carbon. In this work, we explore the use of nitrogen doped carbon in the cathode of a solid-state lithium–oxygen cell. The roles of porosity and surface area of nitrogen doped carbon on electrochemical performance of the lithium–oxygen cell are investigated.

2. Experimental details

Commercially available Ketjenblack (KB) EC 600JD and Calgon activated (CA) carbon were washed with 6M HCl to remove metal impurities. The carbon materials were then rinsed several times with de-ionized (DI) water to remove chlorides and other impurities. The pre-washed carbon was refluxed with 70% HNO_3 over night, rewashed in DI water followed by drying in an oven at 100 °C. Nitrogen doped carbon materials were prepared at an elevated temperature as reported in literature [25,26]. This sample was then employed for further investigations.

Morphologies of the KB, CA, and blend of KB and CA (hereafter referred as C) carbon as well as the nitrogen doped KB (N-KB), nitrogen doped CA (N-CA) and nitrogen doped blend of KB and CA (hereafter referred as N–C) carbon were examined using SEM. Elemental content in the carbon samples were analyzed with energy dispersive X-ray (EDX) spectroscopy. X-ray diffraction (XRD) patterns were collected between 15° and 80° (Rigaku D/MAX) fitted with CuKα radiation source. The Brunauer–Emmett–Teller (BET) surface areas of the carbon materials were obtained using a nitrogen sorption instrument (Micromeritics, ASAP 2020). Samples were degassed for 4 h at 250 °C under vacuum before surface area measurements. The porosity of cathode material was measured using a gas pycnometer (Micromeritis, Accu Pyc II 1340). Thermal stability of these carbon materials were investigated with a thermogravimetric analysis (TGA) system (TA Instruments, model 2050) ramped to 900 °C at heating rate of 5 °C min^{-1} in air. Cyclic voltammetry (CV) measurements were carried out in a standard three-electrode cell configuration with 0.1 M KOH as the electrolyte using a Solartron SI 1287 electrochemical analyzer with scan rate of 5 mV min^{-1}. Pastes consisting of KB and Nafion (tetrafluoroethylene based fluoropolymer-copolymer) solution in one case and N-KB and Nafion in another were prepared and spread on graphite, which was used as the working electrode. A Pt wire was used as the counter electrode and a saturated calomel electrode (SCE) electrode was used as the reference electrode. All potentials are measured with respect to SCE.

Carbon air cathode was fabricated using a procedure reported previously [16]. Briefly, a mixture of N-KB and N-CA carbon powder in a 40:60 wt.% ratio with a polytetrafluoroethylene (PTFE) suspension was ball-milled for an hour. The carbon powder and PTFE were mixed with DI water to obtain a soft mass, which was spread on a nickel foam, used as a current collector, and pressed by sandwiching between two stainless steel plates at 1 MPa. The obtained cathode specimen was dried at 100 °C overnight. A solid-state lithium–oxygen cell with a 2 cm^2 area was fabricated in a commercially available cell casing under a dry argon atmosphere. The N–C film on nickel foam was used as a working cathode, lithium metal as anode and polymer-coated lithium aluminum germanium phosphate (LAGP) as electrolyte. The processing and properties of the LAGP material have been reported and described in our earlier work [27]. Electrochemical performance of the prepared lithium–oxygen cell was examined using a Solartron SI 1287 electrochemical analyzer in conjunction with a SI 1260 Impedance/gain-phase analyzer.

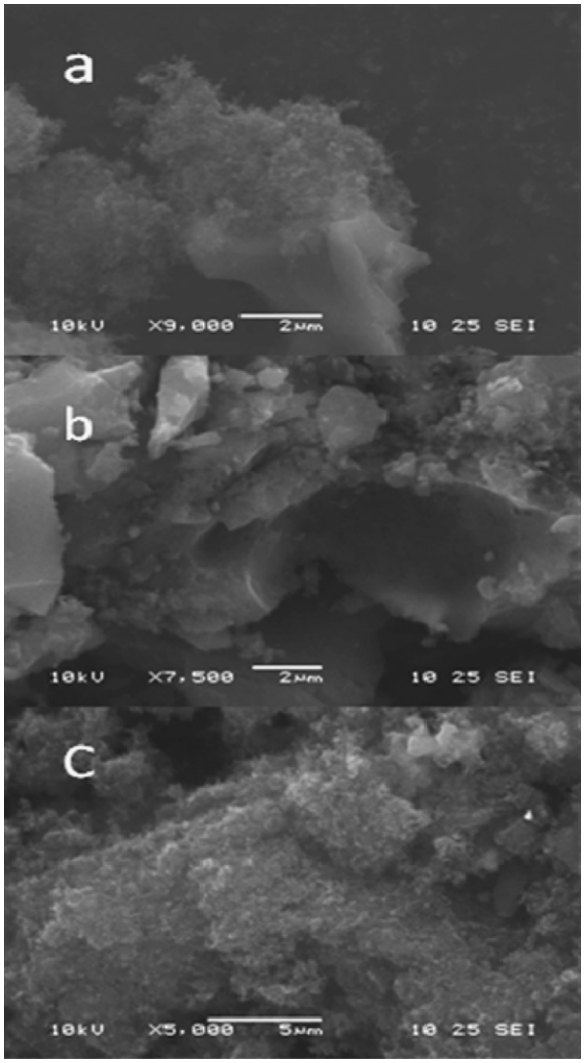

Fig. 1. SEM images of nitrogen doped carbon. (a) Nitrogen doped Ketjenblack (N-KB) carbon, (b) nitrogen doped Calgon activated (N-CA) carbon, and (c) nitrogen doped blend of KB and CA (N–C) carbon.

Charge–discharge measurements on this cell were performed in a galvanostatic mode. Electrochemical impedance spectroscopy (EIS) of the lithium–oxygen cell was conducted over a frequency range 0.1 Hz–10^6 Hz after the charge–discharge cycle. All measurements were carried out under oxygen atmosphere.

3. Results and discussion

Fig. 1 shows the high magnification SEM images of N-KB, N-CA, and N–C carbons.

Fig. 1a reveals the presence of highly dense fibrous and/or spherical carbon in N-KB carbon. It appears from the SEM micrograph that these fibrous carbons are attached with graphitic flakes. Shown in Fig. 1b is the morphology of N-CA carbon revealing flakes or plates like structures. The morphology of the N–C carbon (Fig. 1c) exhibits both the fibrous and plate like structures. EDX analysis was employed to characterize nitrogen contents in these carbons. The EDX conducted on N-KB, N-CA as well as N–C carbons revealed the nitrogen content to be in the range 5–7 at.% (Table 1).

Effect of nitrogen doping in carbons on the micro-structural and electro-catalytic properties was further evaluated by XRD, TGA and CV techniques. XRD patterns for KB and N-KB carbons are shown in Fig. 2a.

Table 1
Physical and structural parameters of various carbon materials.

	Carbon						
	KB	N-KB	CA	N-CA	C	N–C	Cathode with N–C
Surface area ($m^2\ g^{-1}$)	1123	1664	1025	1132	1366	1385	903
Pore volume ($cm^3\ g^{-1}$)	1.2	2.5	0.6	0.7	1.6	1.8	1.1
Pore sze (nm)	4.5	6	2.4	2.4	4.5	4.8	4.6
Porosity (%)	39	44	69	71	38	42	25
TGA (carbonization Temp. °C)	495	521	548	537	553	545	–
EDX (at.%)	0	6.7	0	5.3	0	5.2	–

The XRD spectra of these carbons reflect one prominent peak around 23° and a weak peak at 44° corresponding to the (0 0 2) and (1 0 0) planes of graphite, respectively. The reflection (0 0 2) around 23° indicates the presence of a small domain with parallel stacking of graphene sheets. While the reflection (1 0 0) around 44° is attributed to the fibrous/spherical structures formed by sp^2 hybridized carbons as evident from SEM micrograph. The XRD spectrum exhibits a small shift in the (1 0 0) reflection for N-KB carbon and this shift is due to the incorporation of nitrogen in the carbon. There was no observable shift in the (0 0 2) plane. The TGA analysis was conducted in air for KB and N-KB carbon. No remarkable weight loss or gain was observed (Fig. 2b) in sample mass at temperatures below 490 °C. Significant mass loss occurs at about 495 °C and 521 °C for KB and N-KB carbon, respectively. This is attributed to the thermal oxidation of carbon powder in air involving breakage of C–C and C–N bonds. Above 680 °C, the carbon is fully decomposed. TGA shows higher decomposition temperature for N-KB carbon in comparison to KB carbon, which demonstrates that N-KB carbon possess high thermal stability. This may be due to incorporation of nitrogen in carbon, wherein nitrogen containing groups are linked to carbon structures and this induces a highly stable structure.

The CV of the KB and N-KB carbon in air saturated aqueous solution of 0.1 M KOH (Fig. 2c) reveals a weak oxygen reduction reaction (ORR) activity along the negative scan direction around 0.6 V vs SCE (shown by arrow in Fig. 2c) for N-KB, whereas no clear ORR activity was observed for KB carbon. The broad oxygen reduction signal for N-KB carbon is due to the presence of low concentration of dissolved oxygen in air saturated aqueous solution of 0.1 M KOH solution. Compared to KB carbon, the N-KB carbon exhibits one order of higher magnitude difference in reduction current at potential of 0.6 V along the negative scan direction.

The BET nitrogen adsorption–desorption isotherms of KB, CA and C carbons as well as N-KB, N-CA, and N–C carbons used in the air cathode were obtained.

Shown in Fig. 3a is a typical nitrogen adsorption isotherm for the C as well as N–C carbons. Both isotherms exhibit adsorption hysteresis indicating the presence of mesopores. There is a vertical shift in the location of hysteresis loop to higher volumes of nitrogen gas adsorption for N–C carbon indicating the enhancement in porosity in this carbon. BET surface area, pore volume, pore size, and porosity values of KB, CA, C carbons as well as N-KB, N-CA and N–C carbons were determined and are summarized in Table 1. The remarkable nitrogen uptake above the relative pressure ratio of 0.80 was observed in BET isotherm (Fig. 3a) and is due to the condensation of nitrogen in a mesoporous carbon. The mesopore size distributions of C and N–C carbons are shown in Fig. 3b. The pore size distributions were derived using the BJH (Barrett–Joyner–Halenda) method. Fig. 3b shows the pore size distribution curves for both samples are centered at the 9.5, 12.5 and 42 nm pore diameter. Nitrogen enrichment of C carbon preserves the mesostructure of C carbon as shown in Fig. 3b. Compared to the C carbon, a narrow pore size distribution at 42 nm has been observed for N–C carbon. The high porosity in N–C carbon helps to improve the cell capacity of lithium–oxygen battery as described in the oxygen diffusion model that predicts the cathode pore radius is reflective of the distribution of the lithium peroxide product formed in the cathode during the cell discharge [28]. It is observed from Table 1 that KB carbon has high surface area, while CA carbon has high porosity. Our rationale for using a C carbon was to take advantage of the high surface area of KB carbon and high porosity of CA carbon. It is seen from Table 1 that there is an enhancement of porosity for the nitrogen doped carbons and this facilitates more efficient access to gaseous molecules than those of the undoped carbons. BET measurements on the cathode composed of N–C carbon free standing films show a loss in surface area and porosity that is due to the presence of PTFE component of the air cathode.

The lithium–oxygen cells composed of the C and the N–C carbons as active material in the cathode were fabricated (Fig. 4a) to study their electrochemical performance under oxygen atmosphere. A solid electrolyte laminate reported in our previous work [16] was used to couple the lithium anode with an oxygen cathode. This electrolyte provides very high lithium–ion conductivity, passivates the lithium surface, and enhances lithium–electrolyte interfacial stability. Fig. 4b shows the portion of discharge–charge behavior of the lithium–oxygen cells with cathode fabricated with a C and N–C carbons at the low discharge current of 0.05 mA at 75 °C. It is noticed from the Fig. 4b that at the discharge current of 0.05 mA, the operating cell voltage initially fluctuates for the C carbon cathode. The voltage fluctuation during discharge process remains relatively constant around 2.5 V and reflects existence of interfacial flaws and improper processing of the cell. During the conditioning cycle, sometimes such transient behavior of the cell is noted. Variations of the cell voltage against cell capacity of cathode show flat discharge profile from 2.55 to 2.75 V. The values of open circuit voltage (OCV) were 3.18 V and 2.45 V for N–C and C carbon cathode, respectively. Fig. 4b shows that at the cell capacity of 0.1 mAh, the cell voltage is higher by 0.25 V and 0.38 V for N–C carbon during discharge and charge process, respectively.

Fig. 4c exhibits the discharge capacities of the lithium–oxygen cells with cathode composed of the C and N–C carbons at the discharge current of 0.2 mA at 75 °C. It is observed from Fig. 4c that the cell composed of N–C carbon delivers two times higher cell capacity of 1.44 mAh at a discharge current of 0.2 mA, while a cell capacity of 0.7 mAh was obtained at a discharge current of 0.2 mA for the lithium–oxygen cell with cathode composed of the C carbon. An increase in the cell capacity of the lithium–oxygen cell with cathode composed of the N–C carbon in this work is ascribed to the higher electrocatalytic activity of N–C carbon that helps facilitate the cathodic reactions in lithium–oxygen cell. Apart from higher activity of the N–C carbon, the electrochemical performance of the lithium–oxygen cell also depends on the porosity of the air electrode. Higher porosity of the N–C carbon improves higher oxygen diffusivity in N–C carbon that enhances the cell capacity. It is seen from Fig. 4c that the initial high OCV and its rapid drop for the lithium–oxygen cell with cathode fabricated with N–C carbon might be associated to the cell impurities and residual moisture that could lead to parasitic reactions occurring at the cathode–electrolyte interface. Although, the OCV of lithium–oxygen cell fabricated with N–C cathode is high, there is

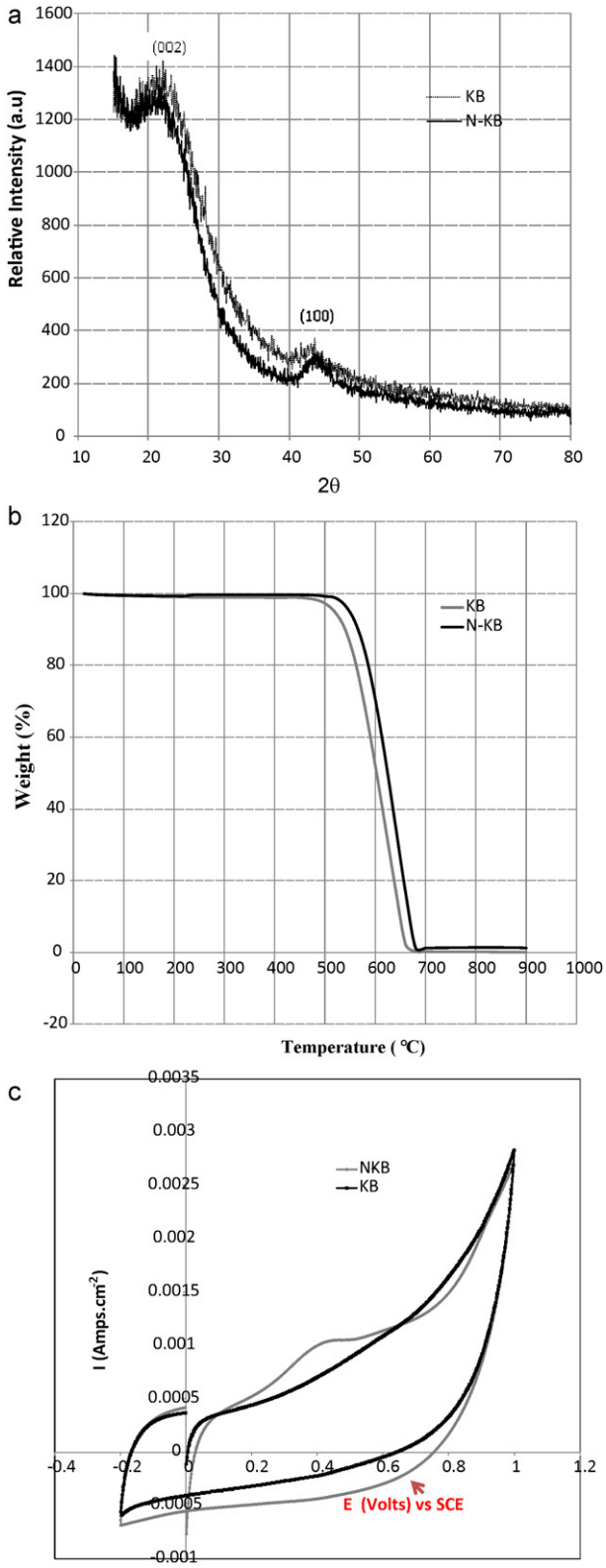

Fig. 2. (a) XRD patterns of Ketjenblack (KB) carbon and nitrogen doped KB carbon (N-KB), (b) TGA of KB and N-KB carbon and (c) CV of KB and N-KB carbon.

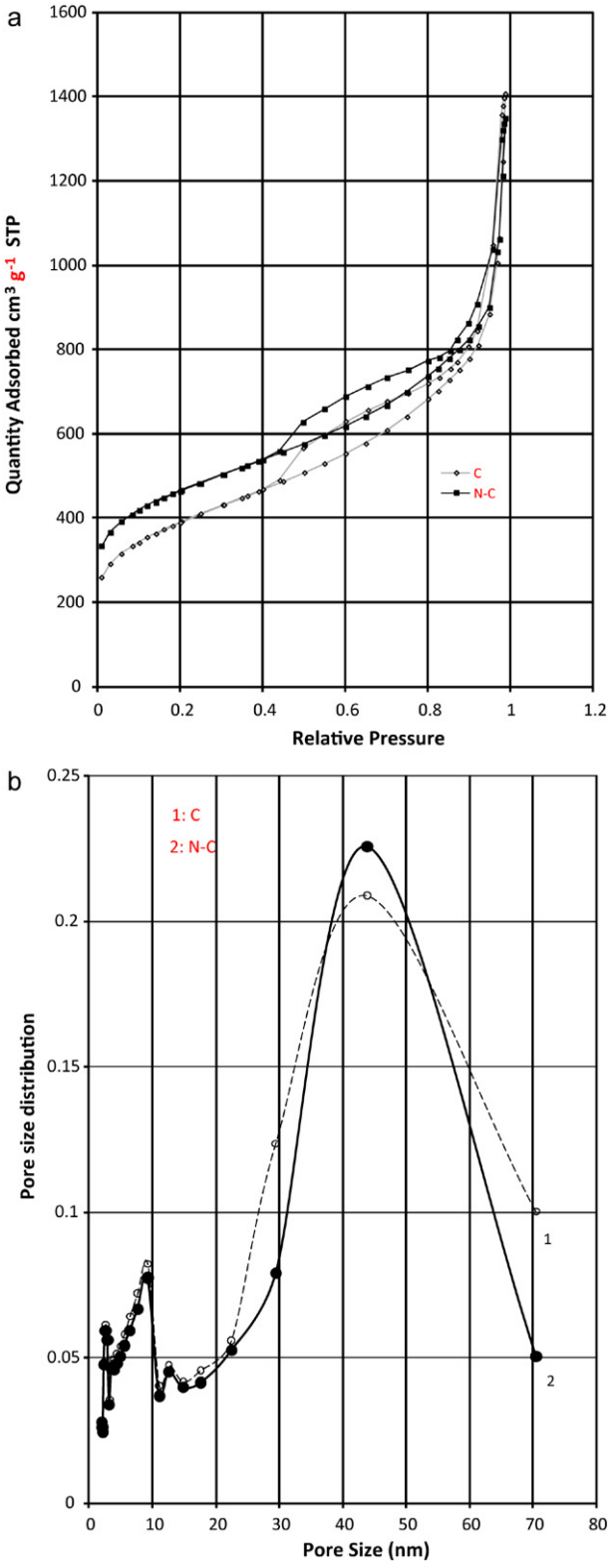

Fig. 3. (a) N_2 adsorption–desorption isotherms for the blend of KB and CA (C) and nitrogen doped blend of KB and CA (N–C) carbon and (b) corresponding pore size distributions for the C and N–C carbon calculated by BJH method.

no benefit of this OCV as it drops down quickly to 2.5 V. However, the role of nitrogen doping in carbon and the parasitic reactions at the cathode–electrolyte interface on the OCV of lithium oxygen cell is not clear and it is of fundamental interest to investigate how nitrogen doping in carbon affects the OCV of these cells. Further work will be carried to understand the role of these parameters. A flat discharge plateau around 2.5 V is also observed in Fig. 4c for the N–C carbon. Such type of flat plateau has been reported for lithium–oxygen cell when discharged in oxygen atmosphere that involve formation of Li_2O_2 and/or Li_2O by the oxidation of metallic

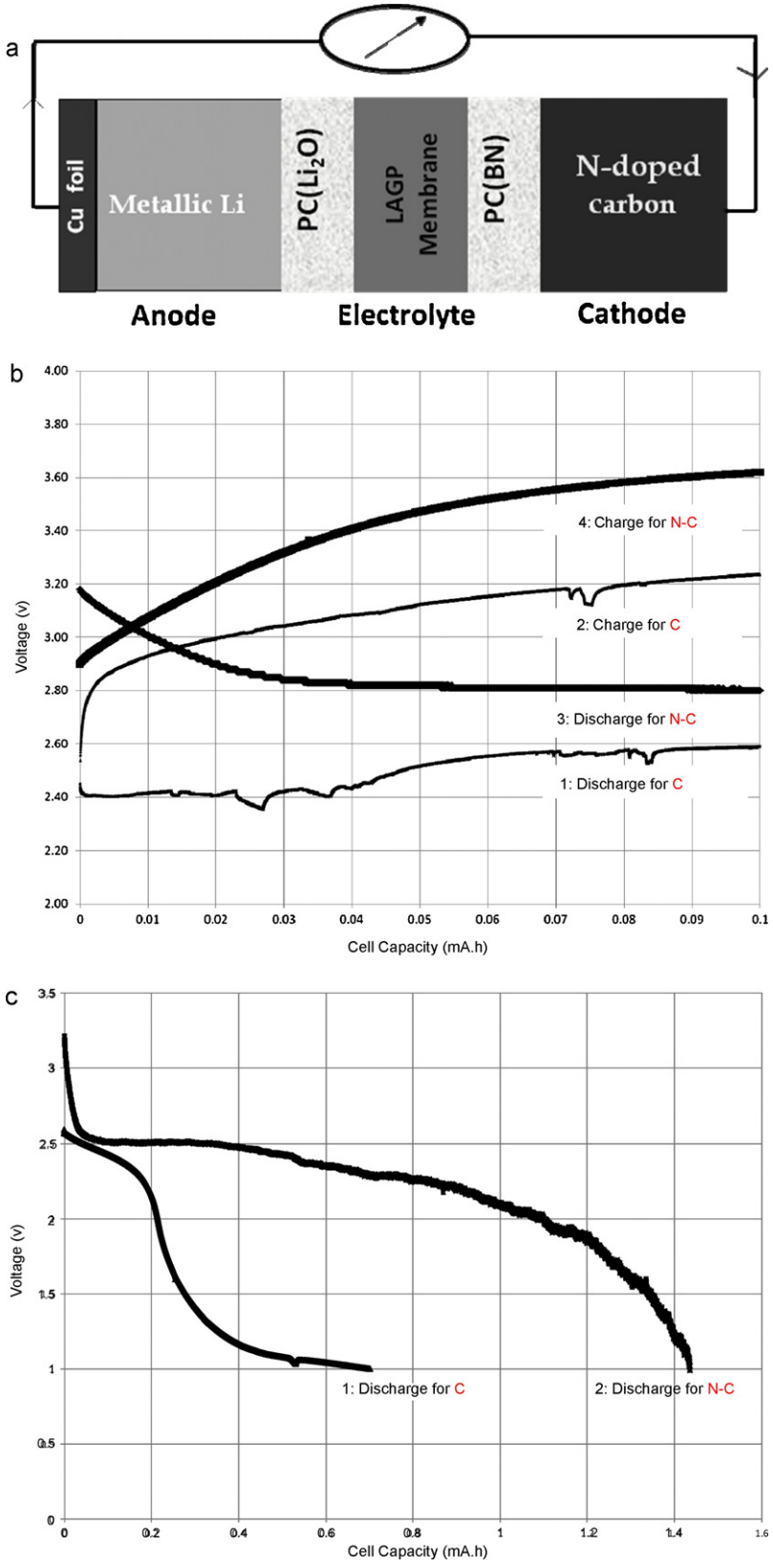

Fig. 4. (a) Schematic representation of lithium–oxygen battery showing lithium anode with three layer membrane laminate, polymer ceramic PC + Li_2O/LAGP(lithium aluminum germanium phosphate) + BN, and N-doped blend of KB and CA (N–C) cathode, (b) discharge–charge curves of lithium–oxygen battery with a constant current of 0.05 mA for the blend of KB and CA (C) carbon (1: discharge and 2: charge) and N–C carbon (3: discharge and 4: charge) at 75 °C and (c) discharge curve of lithium–oxygen cell with discharge current of 0.2 mA at 75 °C for the C (1) and N–C (2) carbon.

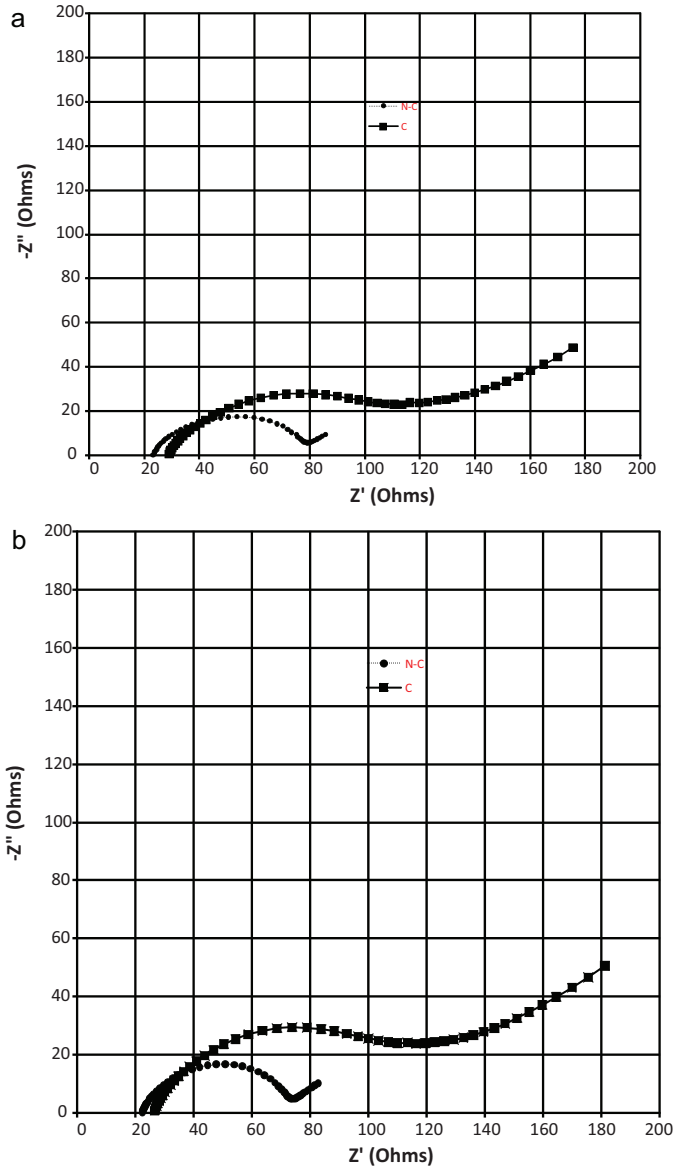

Fig. 5. Nyquist impedance plots of lithium–oxygen cell (a) before discharge of cell and (b) after discharge of cell.

Li [5,6,16,29,30]. The lower cell capacity value for the C carbon is due to lower porosity in cathode to accommodate the discharge products that fill the pores of the cathode and increases the polarization. This is one of the factors that affects the progress and magnitude of discharge reactions.

EIS was used to investigate the electrochemical performance of cathode in the lithium–oxygen cell. The impedance of the lithium–oxygen cell was measured before and after discharge. Typical Nyquist plots in the frequency range from 0.1 Hz to 1 MHz for the C and N–C carbons are shown in Fig. 5a and b.

All plots exhibit a semicircle and a tail. The high frequency intercept on the *Z'* axis corresponds to the resistance of the cell which includes contributions from the electrodes, electrolyte, and contact resistance. The numerical value of width of semicircle on the *Z'* axis corresponds to the charge-transfer resistances and indicates the overall kinetic effects. A tail in the low frequency region represents the characteristics of a diffusion controlled process due to the diffusion of lithium ions and oxygen in the cathode [31,32]. From the Nyquist plots obtained after discharge, the values of diameter were determined to be 130 Ω and 55 Ω for the C and N–C carbon, respectively. Nyquist plots exhibit a higher charge-transfer resistance for the C carbon pointing to slower charge-transfer kinetics. It is observed from these Nyquist plots that the apparent diameter of semicircle of the lithium–oxygen cell fabricated with N–C carbon is smaller than the lithium–oxygen cell fabricated with the C carbon. The decrease by almost half in the charge-transfer resistance of the cathode prepared from the N–C carbon indicates the faster charge-transfer kinetics on cathode made from N–C carbon. A high charge-transfer resistance of air cathode fabricated with C carbon is attributed to the formation of discharge products in the pores of the cathode. EIS analysis suggests that the major contribution to the cell resistance is the charge-transfer resistance, indicating thereby the nitrogen doping suppresses charge-transfer resistance and improves the ORR, as evidenced from Fig. 5a and b. In addition, at discharge currents of 0.05 and 0.2 mA, there is an increase in cell capacity of lithium–oxygen cell prepared with N–C carbon relative to the capacity of cell with C carbon. Both of these studies lead to the conclusion that the nitrogen doping in carbon helps the kinetics of ORR on the oxygen cathode, thereby improving the cell capacity of lithium–oxygen battery. Further studies on the dependence of discharge current on voltage and cell capacity for the cathode prepared from N–C carbon are being investigated.

4. Conclusion

This paper demonstrated that the nitrogen doping of the C carbon significantly improved cell performance of lithium–oxygen battery. The improvement in the cell capacity is attributed to higher surface area, porosity and electrocatalytic activity of N–C carbon. By comparison with the C carbon, the N–C carbon provides a promising approach and suggests a potential for operating in lithium–oxygen battery platforms.

Acknowledgement

This research was supported by the Air Force Research Laboratory, Wright-Patterson Air Force Base, OH, USA.

References

[1] M. Armand, J.M. Tarascon, Nature 451 (2008) 652–657.
[2] G. Girishkumar, B. McCloskey, A.C. Luntz, S. Swanson, W. Wilcke, J. Phys. Chem. Lett. 1 (2010) 2193–2203.
[3] F.T. Wagner, B. Lakshmanan, M.F. Mathias, J. Phys. Chem. Lett. 1 (2010) 2204–2219.
[4] D. Linden (Ed.), Handbook of Batteries Fuel Cells, Mc-Graw-Hil, New York, 1984 (Chapter 38).
[5] K.M. Abraham, Z. Jiang, J. Electrochem. Soc. 143 (1996) 1–5.
[6] J. Read, J. Electrochem. Soc. 153 (2006) A96–A100.
[7] A. Dobley, C. Morein, K. Abraham, The 208th Meeting of the Electrochemical Society, vol. 2005-2, Los Angeles, CA, October 16–21, 2005.
[8] T. Kuboki, T. Okuyama, T. Ohsaki, N. Takami, J. Power Sources 146 (2005) 766–769.
[9] S.D. Beattie, D.M. Manolescu, S.L. Blair, J. Electrochem. Soc. 156 (2009) A44–A47.
[10] T. Ogasawara, A. Debart, M. Holzapfel, P. Novak, P.G. Bruce, J. Am. Chem. Soc. 128 (2006) 1390–1393.
[11] A. Debart, J. Bao, G. Armstrong, P.G. Bruce, J. Power Sources 174 (2007) 1177–1182.
[12] M. Eswaran, N. Munichandraiah, L.G. Scanlon, Electrochem. Solid State Lett. 13 (2010) A121–A124.
[13] J. Xiao, D. Wang, W. Xu, D. Wang, R.E. Williford, J. Liu, J.G. Zhang, J. Electrochem. Soc. 157 (2010) A487–A492.
[14] T. Zhang, N. Imanishi, Y. Shimonishi, A. Hirano, Y. Takeda, O. Yamamoto, N. Sammes, Chem. Commun. 46 (2010) 1661–1663.
[15] Y.-C. Lu, Z. Xu, H.A. Gasteiger, S. Chen, K.H. Schifferli, Y. Shao-Horn, J. Am. Chem. Soc. 132 (2010) 12170–12171.
[16] B. Kumar, J. Kumar, R. Leese, J.P. Fellner, S.J. Rodrigues, K.M. Abraham, J. Electrochem. Soc. 157 (2010) A50–A54.
[17] X. Wang, X. Li, L. Zhang, Y. Yoon, P.K. Weber, H. Wang, J. Guo, H. Dai, Science 324 (2009) 768.
[18] J. Ozaki, N. Kimura, T. Anahara, A. Oya, Carbon 45 (2007) 1847–1853.
[19] B.L. Allen, P.D. Kichambare, A. Star, ACS Nano 2 (2008) 1914–1920.
[20] Z. Lei, M. Zhao, L. Dang, L. An, M. Lu, A.Y. Lo, N. Yu, S.B. Liu, J. Mater. Chem. 19 (2009) 5985–5995.

[21] B. Choi, H. Yoon, I.S. Park, J. Jang, Y.E. Sung, Carbon 45 (2007) 2496–2501.
[22] J.I. Ozaki, S.I. Tanifuji, A. Furuichi, K. Yabutsuka, Electrochim. Acta 55 (2010) 1864–1871.
[23] K. Gong, F. Du, Z. Xia, M. Dustock, L. Dai, Science 323 (2009) 760–764.
[24] Y. Tang, B.L. Allen, D.R. Kauffman, A. Star, J. Am. Chem. Soc. 131 (2009) 13200–13201.
[25] M. Kawaguchi, S. Yagi, H. Enomoto, Carbon 42 (2004) 345–350.
[26] R.J.J. Jansen, H. van Bekkum, Carbon 33 (1995) 1021–1027.
[27] B. Kumar, D. Thomas, J. Kumar, J. Electrochem. Soc. 156 (2009) A506–A513.
[28] S.S. Sandhu, J.P. Fellner, G.W. Brutchen, J. Power Sources 164 (2007) 365–371.
[29] M. Mirzaeian, P.J. Hall, J. Power Sources 195 (2010) 6817–6824.
[30] J.S. Hummelshoj, J. Blomqvist, S. Datta, T. Vegge, J. Rossmeisl, K.S. Thygesen, A.C. Luntz, K.W. Jacobsen, J.K. Norskov, J. Chem. Phys. 132 (2010) 071101-1–171101-4.
[31] E. Barsoukov, J.R. Macdonald (Eds.), Impedance Spectroscopy: Theory, Experiment, and Applications, 2nd ed., John Wiley and Sons, Hoboken, NJ, 2005.
[32] J. Kumar, S.J. Rodrigues, B. Kumar, J. Power Sources 195 (2010) 327–334.